Received 6 December 2023; revised 26 February 2024; accepted 25 March 2024. Date of publication 1 April 2024; date of current version 18 April 2024.

Digital Object Identifier 10.1109/OJCOMS.2024.3383593

Discrete-Time Models and Performance of Phase Noise Channels

AMINA PIEMONTESE [1,2] (Member, IEEE), GIULIO COLAVOLPE [1,2] (Senior Member, IEEE), AND THOMAS ERIKSSON [3]

[1]Department of Engineering and Architecture, University of Parma, 43121 Parma, Italy

[2]CNIT Research Unit, University of Parma, 43121 Parma, Italy

[3]Department of Electrical Engineering, Chalmers University of Technology, 412 96 Gothenburg, Sweden

CORRESPONDING AUTHOR: A. PIEMONTESE (e-mail: amina.piemontese@unipr.it)

This work was supported in part by the European Union under the Italian National Recovery and Resilience Plan (NRRP) of NextGenerationEU, with particular reference to the PRIN 2022 Project 2022BEXMXN titled "INSPIRE: Integrated Terrestrial/Space Wireless Networks for Broadband Connectivity and IoT Services" funded by the Italian MUR.

ABSTRACT This paper deals with the phase noise affecting communication systems, where local oscillators are employed to obtain reference signals for carrier and timing synchronizations. The most common discrete-time phase noise channel model is analyzed, with the aim to fill the gap between measurements and analytical models. In particular, the power loss and the intersymbol interference due to the presence of phase noise is evaluated with reference to the measurements parameters and to the system bandwidth. Moreover, the impact on the communication systems' performance of the phase noise originating from the oscillator non-idealities is considered, in case of free-running and phase-locked oscillators. The proposed analysis allows to extrapolate useful information about the performance of practical systems by investigating the power spectral density of the oscillator phase noise. An expression for the variance of the residual phase error after tracking, which depends on the main parameters of practical oscillators, is derived, and used to study the dependence of the performance on the symbol rate.

INDEX TERMS Phase noise, oscillator noise, phase-locked loop, Wiener process.

I. INTRODUCTION

THE PHASE noise (PN) remains one of the main limiting factors for communication systems. PN due to instabilities of local oscillators, both at the transmitter and at the receiver, can in fact cause a severe performance degradation. Ideally, a local oscillator would produce a sinusoidal signal, whose power spectrum is a delta function at the carrier frequency, but in reality its output power appears also in a band around the desired frequency. Since the PN can strongly limit the performance, the study of the PN effects in communication systems has attracted a lot of interest in the literature of the last decades, see, e.g., [1], [2], [3], [4], [5], [6], [7], [8], [9].

In [10], a PN spectrum model which is very suitable for theoretical calculations is studied. The considered power spectral density (PSD) has the fundamental features typical of the PSD of practical oscillators, i.e., a -20 dB/decade slope, a flat part at low frequencies, representing the attenuation of the PN stabilized by means of a phase-locked loop (PLL), and another flat part at high frequencies. Moreover, it has the Wiener model as a special case. It is similar to other models in the literature [11], [12], [13], but it improves them since it allows us to describe the PN in terms of measurement parameters of practical oscillators and facilitates closed-form expressions of distortions and performance. Starting from the PN PSD, the PSD of the phasor can be derived and expressed in terms of the parameters of the PN PSD, that are related to the oscillator measurements. In this paper, the analysis is extended to the general case where the flat part of the PN PSD at high frequencies is not negligible and without resorting to the approximation of low PN as usually done in the literature.

Despite the large number of publications on the subject, there are questions that are not concisely answered yet. An

important point regards a largely used discrete-time channel model, that ignores the power loss and the intersymbol interference (ISI) affecting the received symbols due to the PN. The PN process has in fact an infinite bandwidth, and some approximation errors will occur when using a discrete-time model. Further, samples at the output of the matched filter are not a sufficient statistic for detection since the receiver filter is not matched due to the presence of PN. In [14], the effect of filtering on the phase noise is considered by using a multi-sample receiver, in the case of Wiener PN and in the absence of ISI, and in [15] bounds on the signal-to-noise ratio (SNR) penalty are derived for the same scenario. In [16], the ISI is considered and the common discrete-time approximation of the filtered and symbol-rate sampled continuous-time PN is evaluated though simulations. However, to the authors' knowledge, the quantification of these neglected effects in terms of the measurement parameters is missing in the literature.

Another relevant question is how can we relate the performance of phase tracking algorithms to the oscillator measurements? It is of particular interest the dependence of the performance on the white oscillator noise floor. This effect has been recently studied in the literature through an experimental approach [17], [18], but a theoretical analysis is still missing.

In this paper, we give an answer to these questions starting from the aforementioned general analytical model [10], which can describe the PSD of the PN of real oscillators. The main contributions of the paper are the following.

- The approximation errors that the discrete-time representation of the PN suffers from are bounded. For example, to quantify the ISI due to the presence of PN in the case of a free-running oscillator and single carrier modulation, the signal-to-interference (SIR) ratio is derived in closed form as a function of the ratio between the phasor bandwidth and the communication system bandwidth, or, equivalently, as a function of the innovation variance σ_u^2 of the discrete-time Wiener PN process. Interestingly, we can find a limit on σ_u to have a SIR higher than a given value, e.g., the SIR is higher than 25 dB if $\sigma_u < 0.1$ rad, and this means that for many realistic cases those approximation errors are limited. A similar investigation was performed in [19], albeit in this manuscript we give deeper insight and results.
- The study of the performance of phase estimators employed at the receiver side is performed. The PSD of the residual phase error after phase tracking is derived and connected to the main measurement parameters of oscillators, to the system bandwidth and to the variance of the additive noise affecting the communication system. The proposed analysis shows that the performance does not depend monotonically on the symbol rate but there exists an optimal value beyond which performance degrades. To the best of the authors' knowledge, this is the first time that the optimal symbol rate is found in closed form.

The rest of the paper is organized as follows. The adopted statistical model of the PN is described in Section II, while the statistical model of the phasor is given in Section III. Section IV introduces the communication system model. The baseband discrete-time PN channel is analyzed in Section V and the theory about the performance of phase trackers is derived in Section VI. Numerical results are collected in Section VII.

Notation. Given a random process $x(t)$, the PSD and the autocorrelation function are denoted by $S_x(\cdot)$ and $R_x(\cdot)$, respectively. The expectation with respect to the random variable y is denoted by $E_y\{\cdot\}$. Operators $\mathcal{R}\{\cdot\}$ and $\mathcal{I}\{\cdot\}$ are the real and imaginary operators.

II. STATISTICAL MODEL OF THE PHASE NOISE

The PN spectrum of many practical oscillators that can be found from measurements is characterized by a -20 dB/decade slope [10] due to integration of white noise inside the oscillator circuitry, and by two flat parts: one at low frequencies, representing the attenuation of the PN stabilized by means of a PLL, the other at high frequencies, modelling the thermal noise at the oscillator output [5]. Therefore, the PN PSD can be modeled as

$$S_\theta(f) = \frac{10^{10}\ell_{100}^2}{f_{3\text{dB}}^2 + f^2} + \ell_\infty^2. \tag{1}$$

where $f_{3\text{dB}}$ is the 3dB bandwidth, and ℓ_{100}^2 and ℓ_∞^2 are the spectrum levels for $f = 100$ kHz and for high frequencies, respectively. The PSD in (1) is obtained by assuming that $f_{3\text{dB}} \ll 100$ kHz[1] and $\ell_\infty \ll \ell_{100}$. The first term in (1) is the PSD of a first-order autoregressive (AR) process [20], while the flat part at high frequencies dominates when $f > \sqrt{\frac{10^{10}\ell_{100}^2}{\ell_\infty^2} - f_{3\text{dB}}^2}$ [10].

In this work, two limiting cases are considered: a free-running oscillator and a PLL oscillator. In particular, the case $f_{3\text{dB}} \to 0$ is studied, which corresponds to a free-running oscillator. In this case, the PN process is a nonstationary Wiener process with a variance that increases linearly with time; on the other hand, the PN has stationary increments and can be described through the variance of the phase increments. The other case is that of high $f_{3\text{dB}}$, i.e., $f_{3\text{dB}} \gg \pi 10^{10}\ell_{100}^2$, which can represent a PLL oscillator with 3dB-bandwidth $f_{3\text{dB}}$. This condition is easily met in practical PLL oscillators. In fact, the value of the spectrum at 100 kHz, ℓ_{100}^2, is most often between -120 and -80 dBc/Hz, therefore the quantity $\pi 10^{10}\ell_{100}^2$ is in the range $[0.03, 300]$ Hz. Since the PLL bandwidth is typically in the order of 1 kHz or 1-2 decades higher than this value, the condition $f_{3\text{dB}} \gg \pi 10^{10}\ell_{100}^2$ is normally satisfied for PLL

[1] When the condition $f_{3\text{dB}} \ll 100$ kHz does not hold, the PSD can simply be expressed as a function of another spectrum level in the -20 dB/decade region.

TABLE 1. Parameters of typical oscillators.

parameter	range
$f_{3\text{dB}}$	$[10^3, 10^5]$ Hz
ℓ_{100}^2	$[-120, -80]$ dBc/Hz
ℓ_∞^2	< -120 dBc/Hz
$\pi 10^{10}\ell_{100}^2$	$[0.03, 300]$ Hz

oscillators. The range of values of parameters of typical oscillators are reported in Table 1.[2]

The above PSD model can be easily extended to match more involved PSDs by assuming that the PN is given by the sum of independent processes, each described by (1). For example, in the case of PN given by the independent contribution of two processes, the extended model is

$$S_\theta(f) = S'_\theta(f) + S''_\theta(f) \tag{2}$$

where both $S'_\theta(f)$ and $S''_\theta(f)$ are given by (1), with suitable different parameters. This extension is used in Section VII to model the PN that can be found in the 3GPP documents [21], [22].

III. POWER SPECTRAL DENSITY OF THE PHASOR

Since both PN and phasor PSDs are used by industries and studied in the literature [14], [23], [24], the PSD of the random process of the phasor $\phi(t) \triangleq e^{j\theta(t)}$ is here derived. Through simulations, it can be observed that the PSD of the phasor follows the one of the PN at high frequencies. In the literature, see, for example, [23], this is motivated by using the low-PN approximation, i.e.,

$$\phi(t) \simeq 1 + j\theta(t) \tag{3}$$

when $\theta(t)$ is small. However, this approximation is not always met (quite often it is not met in practice, actually), and more exact expressions are derived below.

The PSD of the random process of the phasor can be derived starting from the general model of the PN in (1). We first consider the case where the flat part of the PN PSD at high frequency is negligible, i.e., $\ell_\infty^2 = 0$. Let us define the process $h_\tau(t)$ of the phase increments as

$$h_\tau(t) = \theta(t) - \theta(t-\tau). \tag{4}$$

The process $h_\tau(t)$ is a Gaussian random process [25] with zero mean and variance

$$\sigma_{h_\tau}^2 = \mathrm{E}\{(\theta(t) - \theta(t-\tau))^2\} \tag{5}$$

$$= \frac{2\pi 10^{10}\ell_{100}^2}{f_{3\text{dB}}}\left(1 - e^{-2\pi f_{3\text{dB}}|\tau|}\right) \tag{6}$$

where the following expression of the PN autocorrelation

$$R_\theta(\tau) = \frac{\pi 10^{10}\ell_{100}^2}{f_{3\text{dB}}} e^{-2\pi f_{3\text{dB}}|\tau|} \tag{7}$$

obtained by taking the inverse Fourier transform of (1) with $\ell_\infty = 0$, has been used. The variance (6) increases with $|\tau|$ up to a ceiling at $\frac{2\pi 10^{10}\ell_{100}^2}{f_{3\text{dB}}}$. The autocorrelation of the phasor, denoted by $R_\phi(\tau)$, is

$$R_\phi(\tau) = \mathrm{E}\{e^{j\theta(t)}e^{-j\theta(t-\tau)}\} \tag{8}$$

$$= \mathrm{E}\{e^{jh_\tau(t)}\} \tag{9}$$

$$= e^{-\frac{\sigma_{h_\tau}^2}{2}} \tag{10}$$

where the fact that $h_\tau(t)$ is a zero-mean Gaussian random variable has been used. Replacing (6) in (10), the autocorrelation of the phasor process is obtained as

$$R_\phi(\tau) = e^{-\frac{\pi 10^{10}\ell_{100}^2}{f_{3\text{dB}}}\left(1 - e^{-2\pi f_{3\text{dB}}|\tau|}\right)}. \tag{11}$$

The PSD of the phasor process is obtained by taking the Fourier transform of the autocorrelation function

$$S_\phi(f) = e^{-\frac{\pi 10^{10}\ell_{100}^2}{f_{3\text{dB}}}}\delta(f) + e^{-\frac{\pi 10^{10}\ell_{100}^2}{f_{3\text{dB}}}}\int_{-\infty}^{\infty}\left(e^{\frac{\pi 10^{10}\ell_{100}^2 e^{-2\pi f_{3\text{dB}}|\tau|}}{f_{3\text{dB}}}} - 1\right)\cos(2\pi f\tau)\mathrm{d}\tau$$

where $\delta(f)$ denotes the Dirac delta function.

Now the two limiting cases $f_{3\text{dB}} \to 0$ and $f_{3\text{dB}} \gg \pi 10^{10}\ell_{100}^2$ are considered. In the first case, using the approximation $e^{-2\pi f_{3\text{dB}}|t|} \simeq 1 - 2\pi f_{3\text{dB}}|t|$, which is valid when $f_{3\text{dB}} \to 0$, the phasor PSD becomes

$$S_\phi(f)_{f_{3\text{dB}}\to 0} = \mathcal{F}\{e^{-2\pi^2 10^{10}\ell_{100}^2|\tau|}\} = \frac{10^{10}\ell_{100}^2}{\pi^2 10^{20}\ell_{100}^4 + f^2}. \tag{12}$$

When $f_{3\text{dB}} \gg \pi 10^{10}\ell_{100}^2$, the autocorrelation of the phasor can be approximated as

$$R_\phi(\tau) \simeq 1 - \frac{\pi 10^{10}\ell_{100}^2}{f_{3\text{dB}}}\left(1 - e^{-2\pi f_{3\text{dB}}|\tau|}\right) \tag{13}$$

and the PSD can be computed as

$$S_\phi(f)_{\text{high}f_{3\text{dB}}} = \mathcal{F}\left\{1 - \frac{\pi 10^{10}\ell_{100}^2}{f_{3\text{dB}}} + \frac{\pi 10^{10}\ell_{100}^2 e^{-2\pi f_{3\text{dB}}|\tau|}}{f_{3\text{dB}}}\right\} = \left(1 - \frac{\pi 10^{10}\ell_{100}^2}{f_{3\text{dB}}}\right)\delta(f) + \frac{10^{10}\ell_{100}^2}{f_{3\text{dB}}^2 + f^2}. \tag{14}$$

Expressions (12) and (14) give the PSD in the case of a free-running oscillator and in the case of a PLL oscillator, respectively. The PSD for the free-running oscillator is a Lorentzian spectrum, with the value at 100 kHz given by ℓ_{100}^2 and 3-dB bandwidth equal to

$$f_{3\text{dB},\phi} = \pi 10^{10}\ell_{100}^2 \tag{15}$$

and overlaps with (1) for $f \gg \pi 10^{10}\ell_{100}^2$. In the case of the PLL oscillator, the spectrum has a delta function at $f = 0$, and then follows exactly the PN spectrum (1).

The case $\ell_\infty^2 \neq 0$ is now considered. In the following derivation, the bandwidth B_θ of the white PN is introduced as

[2]Parameter $f_{3\text{dB}}$ is given for PLL oscillators.

a help parameter.[3] Ideally, B_θ can be chosen arbitrarily large. On the other hand, $\ell_\infty^2 B_\theta \ll 1$ is assumed in order to bound the error of the used approximations—see (18). In practical oscillators, the value ℓ_∞^2 is in the order of -120 dBc/Hz or less, therefore, even for large B_θ, the above assumption can be satisfied. The statistical quantities that refer to the case of $\ell_\infty^2 \neq 0$ are marked with a circumflex accent. When the assumption $\ell_\infty^2 = 0$ is removed, the autocorrelation of the phasor is

$$\hat{R}_\phi(\tau) = R_\phi(\tau) e^{-\ell_\infty^2 B_\theta (1-\mathrm{sinc}(\tau B_\theta))} \tag{16}$$

where the autocorrelation of the phasor when $\ell_\infty^2 = 0$, $R_\phi(\tau)$, is given in (11). Using the first order Taylor expansion of the exponential $e^x \simeq 1 + x$ in (16), we get

$$e^{-\ell_\infty^2 B_\theta 1-\mathrm{sinc}(\tau B_\theta)} = 1 - \ell_\infty^2 B_\theta (1 - \mathrm{sinc}(\tau B_\theta)) + E(\tau), \tag{17}$$

where $E(\tau)$ is the approximation error, upper bounded by the second term of the Taylor expansion [26], that is

$$E(\tau) \leq \ell_\infty^4 B_\theta^2 (1 - \mathrm{sinc}(\tau B_\theta))^2/2 \leq \ell_\infty^4 B_\theta^2. \tag{18}$$

As stated, this error is low for a large range of values of B_θ. If, for example, we consider $\ell_\infty^2 = -120$ dB, we have an error smaller than 10^{-4} for $B_\theta < 10^{10}$. For this reason, we neglect $E(\tau)$ in the following. Using (17) in (16), we get

$$\hat{R}_\phi(\tau) = R_\phi(\tau)(1 - \ell_\infty^2 B_\theta + \ell_\infty^2 B_\theta \mathrm{sinc}(\tau B_\theta)) \tag{19}$$

and the PSD of the phasor is obtained by taking the Fourier transform of the above autocorrelation, i.e.,

$$\hat{S}_\phi(f) = (1 - \ell_\infty^2 B_\theta) S_\phi(f) + S_\phi(f) \otimes \ell_\infty^2 \Pi\left(\frac{f}{B_\theta}\right) \tag{20}$$

where symbol $\otimes$ denotes convolution and $\Pi(f)$ is the rectangular function equal to one for $-1/2 < f < 1/2$ and zero otherwise. In (20), the factor $1 - \ell_\infty^2 B_\theta$ that multiplies $S_\phi(f)$ makes the power of the phasor unitary, while the effect of the flat PN, dominating at high frequencies, is represented by the second term, which, in the case of free-running oscillator, is

$$S_\phi(f) \otimes \ell_\infty^2 \Pi\left(\frac{f}{B_\theta}\right) = \frac{\ell_\infty^2}{\pi}\left[\tan^{-1}\left(\frac{1}{\pi 10^{10} \ell_{100}^2}\left(f + \frac{B_\theta}{2}\right)\right) - \tan^{-1}\left(\frac{1}{\pi 10^{10} \ell_{100}^2}\left(f - \frac{B_\theta}{2}\right)\right)\right]. \tag{21}$$

This term is constant and equal to ℓ_∞^2 for $|f| \ll B_\theta$ and equal to zero for $|f| \gg B_\theta$. The function in (21) is shown in Figure 1 for $B_\theta = 10^9$, $\ell_\infty^2 = -130$ dBc/Hz and $\ell_{100}^2 = -90$ dBc/Hz.

Using the approximation $\ell_\infty^2 B_\theta \ll 1$, and assuming that B_θ is larger than the system bandwidth, the PSD of the phasor in the communication band can be written with good approximation as

$$\hat{S}_\phi(f) = S_\phi(f) + \ell_\infty^2. \tag{22}$$

[3]This is necessary to avoid dealing with a white process with infinite bandwidth and power, but the end results are independent of this help parameter.

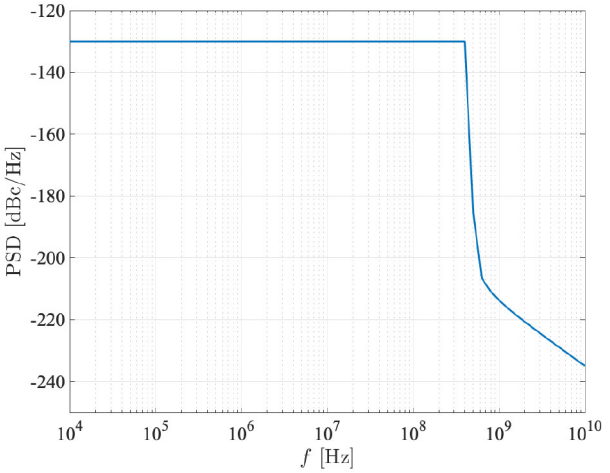

FIGURE 1. Flat part of the phasor power spectral density given in (21), for $B_\theta = 10^9$, $\ell_\infty^2 = -130$ dBc/Hz and $\ell_{100}^2 = -90$ dBc/Hz.

IV. APPLICATION TO COMMUNICATIONS

A communication system is considered, where linearly modulated symbols $\{x_n\}$ are transmitted through the channel. At the receiver, after down-conversion, the received signal is

$$r(t) = \sum_n x_n p(t - nT_\mathrm{s}) e^{j\theta_\mathrm{T}(t)} e^{j\theta_\mathrm{R}(t)} + v(t) e^{j\theta_\mathrm{R}(t)} \tag{23}$$

where T_s is the symbol time, $p(t)$ is the shaping pulse with unitary energy satisfying the Nyquist criterion, $v(t)$ is the complex additive white Gaussian noise (AWGN) with PSD N_0, and $\theta_\mathrm{T}(t)$ and $\theta_\mathrm{R}(t)$ are the PN processes that arise from local oscillator instabilities at the transmitter and at the receiver, respectively (see Section II). The model (23) can be rewritten as

$$r(t) = \sum_n x_n p(t - nT_\mathrm{s}) e^{j\theta(t)} + w(t) \tag{24}$$

where $w(t)$ is an AWGN with same statistics of $v(t)$ and $\theta(t)$ is the sum of transmitter and receiver PN processes. The PSD of $\theta(t)$ is the sum of the PSDs of $\theta_\mathrm{T}(t)$ and $\theta_\mathrm{R}(t)$, since the two PN processes are independent. In many practical cases, receiver and transmitter oscillators have quite different performance, and hence only the dominant PN can be considered, i.e., the PN of the oscillator adopted in consumer grade equipment. In other cases, they are similar and $\theta(t)$ has the sum level of both PNs. Hence, the PSD model described in Section II is applicable in both cases.

At the receiver side, a filter matched to the shaping pulse $p(t)$ is employed, followed by a sampler at symbol time. The received samples represent an approximate sufficient statistic and are given by

$$y_k = r(t) \otimes p^*(-t)_{|_{t=kT_\mathrm{s}}}. \tag{25}$$

The considered system model is shown in Figure 2.

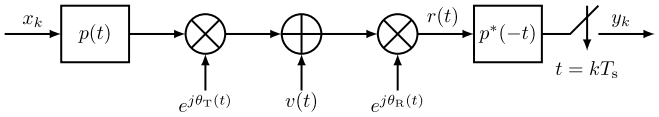

FIGURE 2. Block diagram of the system model.

A commonly studied discrete-time channel model is

$$z_k = x_k e^{j\theta_k} + w_k \tag{26}$$

where θ_k is the PN sample obtained as $\theta_k = \theta(kT_s)$ and w_k is the sample obtained by filtering and sampling the AWGN signal $w(t)$, with variance $\sigma_w^2 = N_0/T_s$. The discrete-time model for the PN with PSD (1) is

$$\theta_k = \theta_k^c + \theta_k^f \tag{27}$$

where θ_k^c and θ_k^f are independent processes, the former inducing the -20 dB/decade slope in the PN PSD, which dominates close-to-carrier, the latter inducing the flat part of the PSD, that dominates at high frequencies. Random variables $\{\theta_k^f\}$ are independent and identically distributed (i.i.d.) zero-mean Gaussian variables with variance $\sigma_f^2 = \ell_\infty^2/T_s$, while θ_k^c is a discrete-time AR random process

$$\theta_k^c = a\theta_{k-1}^c + u_k \tag{28}$$

where u_k are i.i.d. zero-mean Gaussian variables with variance σ_u^2, and parameters a and σ_u^2 are

$$a = e^{-2\pi f_{3\text{dB}} T_s}, \quad \sigma_u^2 = \frac{\pi 10^{10}\ell_{100}^2}{f_{3\text{dB}}}(1 - e^{-4\pi f_{3\text{dB}} T_s}). \tag{29}$$

The aliasing affecting the PSD of the process θ_k^c in the band $[-1/2T_s, 1/2T_s]$ has power

$$\sigma_{\text{alias}}^2 = \frac{\pi 10^{10}\ell_{100}^2}{f_{3\text{dB}}}\left(1 - \frac{2}{\pi}\tan^{-1}\left(\frac{1}{2T_s f_{3\text{dB}}}\right)\right). \tag{30}$$

The case of a free-running oscillator implies that $f_{3\text{dB}} \to 0$. In this case, the parameter a is equal to 1 and the model (28) reduces to the Wiener (random-walk) model. The Wiener process is nonstationary, but the process of the phase increment u_k is stationary and the PN can be described through the variance σ_u^2. We can compute the variance of the phase increments in (29) by taking the limit for $f_{3\text{dB}} \to 0$ and we obtain

$$\sigma_u^2 = 4\pi^2 10^{10}\ell_{100}^2 T_s \tag{31}$$

$$= 4\pi\rho \tag{32}$$

where $\rho \triangleq f_{3\text{dB},\phi}\, T_s$ represents the ratio between the phasor 3-dB bandwidth and the signal bandwidth and will be called *relative bandwidth parameter* in the following.

Model (26) neglects the ISI and the power loss due to the presence of PN. In fact, the PN causes an enlargement of the signal bandwidth, therefore the filter matched to the shaping pulse $p(t)$ cuts some spectral components of the signal, resulting in a power loss. Moreover, the received samples are affected by ISI due to mismatched filters. These effects are quantified in Section V.

V. ERROR ANALYSIS OF THE DISCRETE-TIME CHANNEL

Here, the accuracy of the communication model (26) is evaluated. Thanks to the statistical model described in Section III, the results of this analysis can be connected to the main PN parameters of practical oscillators. The case of a free-running oscillator with $\ell_\infty^2 = 0$ is studied, for which the PSD of the phasor is given by (12). The case $\ell_\infty^2 \neq 0$ is considered at the end of the section.

The following mean square error (MSE) is computed and related to the parameters of the PN

$$\eta = E_{x,\theta,w}\left\{|z_k - y_k|^2\right\} \tag{33}$$

where the expectation is done with respect to the transmitted symbols, the PN and the AWGN. In (33), z_k is the received sample of the simplified model (26) ignoring ISI and power loss, while y_k is the received sample of the more accurate model (25). In order to describe the effect of the PN and matched filtering on the received samples, we define the following linear time-varying discrete filter

$$g_{n,m} = p(t)e^{j\theta(t+mT_s)} \otimes p^*(-t)|_{t=nT_s}. \tag{34}$$

In the absence of PN and for a Nyquist shaping pulse, $g_{0,m} = 1$ and $g_{n,m} = 0$ for $n \neq 0$.

Lemma 1: Consider the system model described in (24), where the phasor $e^{j\theta(t)}$ has PSD given in (12). Let $e^{j\theta_k}$ be the sample $e^{j\theta(kT_s)}$. The MSE in (33) between z_k defined in (26) and y_k defined in (25) is given by

$$\eta = \eta_{\text{D}} + \eta_{\text{ISI}} \tag{35}$$

where

$$\eta_{\text{D}} = E_\theta\left\{|e^{j\theta_k} - g_{0,k}|^2\right\} \tag{36}$$

$$\eta_{\text{ISI}} = \sum_{m\neq 0} E_\theta\left\{|g_{m,k-m}|^2\right\} \tag{37}$$

and the terms $g_{n,m}$ are given in (34).

Proof: By expanding (25), we obtain

$$y_k = \sum_m x_{k-m}g_{m,k-m} + w_k \tag{38}$$

$$= x_k g_{0,k} + \sum_{m\neq 0} x_{k-m}g_{m,k-m} + w_k \tag{39}$$

where $g_{0,k}$ is connected to a power loss of the desired output x_k, and the summation represents ISI. Using (26) and (39) in (33), we obtain

$$\eta = E_{x,\theta}\left\{|x_k e^{j\theta_k} - x_k g_{0,k} - \sum_{m\neq 0} x_{k-m}g_{m,k-m}|^2\right\}.$$

Assuming that the transmitted symbols are zero mean, i.i.d., and with unitary energy, η becomes the sum of two errors,

one due to the approximation of $g_{0,k}$ with the phasor $e^{j\theta_k}$, the other due to the ISI, that is

$$\eta = E_\theta\left\{|e^{j\theta_k} - g_{0,k}|^2\right\} + \sum_{m\neq 0} E_\theta\left\{|g_{m,k-m}|^2\right\}.$$

As expected, in the absence of PN and for a Nyquist shaping pulse, $g_{0,k} = 1$ and $g_{m,k} = 0$ for $m \neq 0$. ■

For convenience, the following terms are defined

$$\gamma_m = E_\theta\{|g_{m,k-m}|^2\} \tag{40}$$

which, using the definition of $g_{n,m}$ in Lemma 1, can be written as

$$\gamma_m = \int_{-\infty}^{+\infty}\int_{-\infty}^{+\infty} p(t)p^*(t_1)p^*(t-mT_s)p(t_1-mT_s) \cdot R_\phi(t_1-t)dtdt_1, \tag{41}$$

where $R_\phi(\tau)$ is the autocorrelation of the phasor $\phi(t) = e^{j\theta(t)}$. Equation (41) shows that the terms γ_m are independent of k. When a detector that is not able to account for the ISI is employed, the SIR can be expressed as a function of the terms γ_m. Using the assumption of zero mean symbols and considering that the symbols are independent, with unitary energy, we have

$$\text{SIR} = \frac{\gamma_0}{\sum_{m\neq 0}\gamma_m}. \tag{42}$$

The following theorem gives the expression of the MSEs in Lemma 1 as a function of the PN parameters and of the system bandwidth. The theory is derived by assuming that the filter $p(t)$ is a root-raised cosine (RRC) shaping pulse with roll-off factor zero, i.e., a normalized sinc function. Other roll-off factors will be considered later in this paper.

Theorem 1: Consider the system model described in (24), where $p(t)$ is the normalized sinc function with unitary energy, and the phasor $e^{j\theta(t)}$ has PSD given in (12), with bandwidth $f_{3\text{dB},\phi}$ (15). The MSEs η, defined in (33), η_D and η_ISI, defined in Lemma 1, are given by

$$\eta = 1 + \frac{2}{\pi}\left[\frac{\rho}{2}\log\left(1+\frac{1}{\rho^2}\right) - \tan^{-1}\left(\frac{1}{\rho}\right)\right] \tag{43}$$

$$\eta_\text{D} = 1 + \frac{2}{\pi}\left[\rho - (1+\rho^2)\tan^{-1}\left(\frac{1}{\rho}\right)\right], \tag{44}$$

$$\eta_\text{ISI} = \frac{2}{\pi}\left[\rho^2\tan^{-1}\left(\frac{1}{\rho}\right) + \frac{\rho}{2}\log\left(1+\frac{1}{\rho^2}\right) - \rho\right] \tag{45}$$

where $\rho = f_{3\text{dB},\phi}\,T_\text{s}$.

Proof: The MSE between the phasor $e^{j\theta_k}$ and $g_{0,k}$ is given in (36). Expanding (36), we obtain

$$\eta_\text{D} = 1 + \gamma_0 - 2\Re\left(E_\theta\left\{e^{-j\theta_k}g_{0,k}\right\}\right), \tag{46}$$

where γ_0 is given in (41) with $m = 0$. First the computation of γ_0 is considered. The expression of the pulse $p(t)$,

$$p(t) = \frac{1}{\sqrt{T_s}}\text{sinc}\left(\frac{t}{T_s}\right) \tag{47}$$

is substituted in (41) with $m = 0$,

$$\gamma_0 = \frac{1}{T_s{}^2}\int_{-\infty}^{+\infty}\int_{-\infty}^{+\infty}\text{sinc}^2\left(\frac{t}{T_s}\right)\text{sinc}^2\left(\frac{t_1}{T_s}\right)R_\phi(t_1-t)dtdt_1, \tag{48}$$

then $R_\phi(t_1 - t)$ is replaced with

$$R_\phi(t_1-t) = \mathcal{F}^{-1}\{S_\phi(f)\,e^{-j2\pi tf}\} = \int_{-\infty}^{+\infty} S_\phi(f)\,e^{j2\pi t_1 f}e^{-j2\pi tf}df$$

and the integrals in (48) are rearranged in the following way

$$\gamma_0 = \frac{1}{T_s{}^2}\int_{-\infty}^{+\infty}\left(\int_{-\infty}^{+\infty}\text{sinc}^2\left(\frac{t}{T_s}\right)e^{-j2\pi tf}dt\right) \left(\int_{-\infty}^{+\infty}\text{sinc}^2\left(\frac{t_1}{T_s}\right)e^{j2\pi t_1 f}dt_1\right)S_\phi(f)\;df. \tag{49}$$

The two internal integrals in t and t_1 equal the Fourier transform of sinc^2, that is

$$\int_{-\infty}^{+\infty}\text{sinc}^2\left(\frac{t}{T_s}\right)e^{-j2\pi tf}dt = T_s\Lambda(fT_s), \tag{50}$$

where $\Lambda(x)$ is the triangular function, i.e., $\Lambda(x) = 1-|x|$, for $-1 < x < 1$ and zero otherwise. Replacing the expression of $S_\phi(f)$ given in (12) in (49), the following expression is obtained

$$\gamma_0 = \frac{2}{\pi}\left[\tan^{-1}\left(\frac{1}{\rho}\right)\left[1-\rho^2\right] - \rho\log\left(1+\frac{1}{\rho^2}\right) + \rho\right] \tag{51}$$

where $\rho = \pi 10^{10}\ell_{100}^2 T_s = f_{3\text{dB},\phi}\,T_\text{s}$. The last term in (46) can be computed as

$$E_\theta\left\{e^{-j\theta_k}g_{0,k}\right\} = \frac{1}{T_s}\int_{-\infty}^{+\infty}\text{sinc}^2\left(\frac{t}{T_s}\right)R_\phi(t)dt = \frac{2}{\pi}\left[\tan^{-1}\left(\frac{1}{\rho}\right) - \frac{\rho}{2}\log\left(1+\frac{1}{\rho^2}\right)\right]. \tag{52}$$

Using (51) and (52) in (46), equation (44) is obtained, concluding the proof for η_D.

Now the computation of η_ISI is considered. Using the definition of γ_m in (40), we can write

$$\eta_\text{ISI} = \sum_{m\neq 0}\gamma_m. \tag{53}$$

In the following, the above summation is computed over all m, then γ_0 in (51) is subtracted to the sum to obtain η_ISI. Signal $r'(t)$ is defined as the received signal without AWGN, i.e.,

$$r'(t) = \sum_n x_n p(t-nT_\text{s})e^{j\theta(t)}. \tag{54}$$

Similarly, $y'(t)$ and y'_k are the signal after matched filtering and the samples after sampling, respectively, without AWGN. The process $r'(t)$ is cycle-stationary, and can be made wide-sense stationary with the classical approach of introducing a random delay, uniformly distributed in $[-T_s, T_s]$. The power of the process $y'(t)$ can be computed by integrating its PSD, that is

$$P_{y'} = \int_{-\infty}^{+\infty} S_{r'}(f)\;|P(f)|^2 df \tag{55}$$

$$= \frac{T_s}{\pi}\int_{-\frac{1}{2T_s}}^{+\frac{1}{2T_s}} \tan^{-1}\left(\frac{f+1/2T_s}{\pi 10^{10}\ell_{100}^2}\right) - \tan^{-1}\left(\frac{f-1/2T_s}{\pi 10^{10}\ell_{100}^2}\right) df \tag{56}$$

$$= \frac{2}{\pi}\left[\tan^{-1}\left(\frac{1}{\rho}\right) - \frac{\rho}{2}\log\left(1+\frac{1}{\rho^2}\right)\right]. \tag{57}$$

In (55), $P(f)$ is the Fourier transform of $p(t)$. In (56), the fact that the PSD of the received signal is given by the convolution of the PSD of the information carrying signal and that of the phasor $e^{j\theta(t)}$ has been used. Since the process $y'(t)$ is bandlimited with bandwidth $1/T_s$, the following relationship holds

$$P_{y'} = E_{x,\theta}\left\{|y'_k|^2\right\} = \sum_m \gamma_m. \tag{58}$$

By using (57) and (58), we obtain

$$\sum_m \gamma_m = \frac{2}{\pi}\left[\tan^{-1}\left(\frac{1}{\rho}\right) - \frac{\rho}{2}\log\left(1+\frac{1}{\rho^2}\right)\right] \tag{59}$$

and from (53) and (51) we get (45). Finally, equation (36) is obtained by using Lemma 1. ■

The expressions above show that the error made when using the channel model (26) depends only on the relative bandwidth parameter. The SIR can be expressed as a function of ρ: starting from (42), the expression of γ_0 in (51) is used in the numerator, while the denominator is η_{ISI}, i.e.,

$$\text{SIR} = \frac{\tan^{-1}\left(\frac{1}{\rho}\right)\left[1-\rho^2\right] - \rho\log\left(1+\frac{1}{\rho^2}\right) + \rho}{\rho^2\tan^{-1}\left(\frac{1}{\rho}\right) + \frac{\rho}{2}\log\left(1+\frac{1}{\rho^2}\right) - \rho}. \tag{60}$$

The SIR can be also expressed as a function of the phase increment standard deviation by using equation (32) which connects ρ with σ_u, i.e.,

$$\text{SIR} = \frac{\tan^{-1}\left(\frac{4\pi}{\sigma_u^2}\right)\left[1-\frac{\sigma_u^4}{16\pi^2}\right] - \frac{\sigma_u^2}{4\pi}\log\left(1+\frac{16\pi^2}{\sigma_u^4}\right) + \frac{\sigma_u^2}{4\pi}}{\frac{\sigma_u^4}{16\pi^2}\tan^{-1}\left(\frac{4\pi}{\sigma_u^2}\right) + \frac{\sigma_u^2}{8\pi}\log\left(1+\frac{16\pi^2}{\sigma_u^4}\right) - \frac{\sigma_u^2}{4\pi}}. \tag{61}$$

From the above equation, a limit on σ_u can be computed to have a SIR higher than a given value. For example, a SIR higher than 25 dB requires $\sigma_u < 0.1$ rad. The extension to the case where ℓ_∞ is not negligible is performed by using equation (22) and we obtain

$$\text{SIR} = \frac{\gamma_0 + \frac{2}{3}\frac{\ell_\infty^2}{T_s}}{\sum_{m\neq 0}\gamma_m + \frac{1}{3}\frac{\ell_\infty^2}{T_s}}. \tag{62}$$

A. IMPACT ON FREQUENCY SELECTIVE CHANNELS

In modern wideband wireless communication standards, OFDM is adopted to cope with frequency selectivity generated by multipath fading. The selection of an OFDM symbol time much lower than the channel coherence time ensures that the use of complex equalization schemes can be avoided. In fact, under this condition, the subcarriers' orthogonality is preserved and a simple single-tap equalizer on each subcarrier is sufficient. When PN comes into play, the picture changes dramatically since it can hardly be considered constant over the OFDM symbol duration. Orthogonality is thus destroyed and ICI appears [1], [2], [3], [23], [27], [28].

The discrete-time model (28) for the PN can be used to compute the signal-to-noise-plus-interference ratio (SINR) in OFDM systems, with the aim of evaluating the impact of PN on ICI. An N-subcarrier OFDM system with symbol period T is considered. The multipath fading channel is assumed to have a delay spread uniformly and independently distributed within the cyclic prefix and channel gains in the frequency domain with unitary energy, as given in [3], [29]. The PN on the kth sample of the generic OFDM symbol is given by the model (28), with $T_s = T/N$. Under the above assumptions, the SINR can be computed in closed form. By following similar steps to [3], where the SINR is given in the case of Wiener PN, the following expression is obtained

$$\text{SINR} = \frac{I(0)}{\sum_{p=1}^{N-1} I(p) + \frac{N^2}{\omega}} \tag{63}$$

where ω is the SNR per subcarrier and

$$I(p) = \sum_{n=0}^{N-1}\sum_{l=n+1}^{N-1} 2\Re\left\{e^{(j2\pi p(n-l)/N - \iota(n,l)\sigma_u^2/2}\right\} + N \tag{64}$$

$$\iota(n,l) = \frac{(a^n-a^l)^2(a^{-2\min(n,l)}-a^2) + 1 - a^{2|n-l|}}{1-a^2}. \tag{65}$$

In (63), $I(0)$ and $\sum_{p=1}^{N-1} I(p)$ account for the common phase error (CPE) and the ICI, respectively. For $a \to 1$, or equivalently $f_{3\text{dB}} \to 0$, the derived expression for the SINR coincides with the one in [3] for the case of Wiener PN.

VI. OPTIMAL PHASE TRACKING THEORY

In this section, we show how to apply the optimal estimation theory in the context of phase tracking. We consider the case where the power loss and the ISI studied in the previous section are negligible, i.e., $y_k \simeq z_k$. This hypothesis is removed in Section VII, where the PN is generated according to the general model (25).

A. AUXILIARY CHANNEL MODELS

The estimator design is based on auxiliary channel models, whose accuracy depends on the SNR. Interestingly, the two models lead to the same expression of the residual PN error after tracking.

1) LOW PN APPROXIMATION

Using the low PN approximation, $e^{j\theta_k} \simeq 1 + j\theta_k$, we get the following relationship

$$\mathcal{I}\{y_k/x_k\} \simeq \theta_k + \mathcal{I}\{w_k/x_k\} \tag{66}$$

We define $d_k^{(1)} = \mathcal{I}\{y_k/x_k\}$ and $n_k^{(1)} = \mathcal{I}\{w_k/x_k\}$ and obtain

$$d_k^{(1)} \simeq \theta_k + n_k^{(1)} \tag{67}$$

where $n_k^{(1)}$ has variance

$$\text{var}(n_k^{(1)}) = \frac{1}{|x_k|^2}\frac{\sigma_w^2}{2}. \tag{68}$$

2) HIGH SNR APPROXIMATION [6]

The modulus of the observable y_k is

$$|y_k| = \left|x_k e^{j\theta_k} + w_k\right| \tag{69}$$

$$= \left||x_k| e^{j\angle x_k} e^{j\theta_k} + w_k' e^{j\angle x_k} e^{j\theta_k}\right| \tag{70}$$

$$= \left||x_k| + w_k'\right| \tag{71}$$

where w_k' is statistically equivalent to w_k. From the above equation, it can be seen that the modulus of the observable cannot be used for the phase estimation. On the other hand, the phase of y_k can be expressed as

$$\angle y_k = \angle\left(x_k e^{j\theta_k} + w_k\right) \tag{72}$$

$$= \angle\left(|x_k| e^{j\angle x_k} e^{j\theta_k} + w_k' e^{j\angle x_k} e^{j\theta_k}\right) \tag{73}$$

$$= \angle x_k + \theta_k + \angle\left(|x_k| + w_k'\right) \tag{74}$$

$$= \angle x_k + \theta_k + \tan^{-1}\frac{\mathcal{I}\{w_k'\}}{|x_k| + \mathcal{R}\{w_k'\}} \tag{75}$$

In the asymptotic case of high SNR, we have

$$\tan^{-1}\frac{\mathcal{I}\{w_k'\}}{|x_k| + \mathcal{R}\{w_k'\}} \simeq \frac{\mathcal{I}\{w_k'\}}{|x_k|}. \tag{76}$$

We define the following auxiliary variable

$$d_k^{(2)} = (\angle y_k - \angle x_k) \mod 2\pi, \tag{77}$$

where the operator $(\cdot) \mod 2\pi$ represents a wrapping of the phase in the interval $[-\pi, \pi)$, and we obtain the second auxiliary channel model

$$d_k^{(2)} \simeq \theta_k + n_k^{(2)} \tag{78}$$

where $n_k^{(2)} = \mathcal{I}\{w_k'\}/|x_k|$ has variance

$$\text{var}(n_k^{(2)}) = \frac{1}{|x_k|^2}\frac{\sigma_w^2}{2}. \tag{79}$$

It is important to note that the two above approximations $d_k^{(1)}$ and $d_k^{(2)}$ lead to the same channel model, being the statistics of the noise in (78) and that in (67) the same. Therefore, they will lead to the same expression of the optimal estimation filter.

In the following, the approximation error of the above models is studied. The exact model can be written as

$$D_k = d_k^{(i)} + e_k^{(i)}, \tag{80}$$

for $i = 1, 2$, where we defined the errors as

$$e_k^{(1)} = \theta_k - \mathcal{I}\left\{e^{j\theta_k}\right\}$$

$$e_k^{(2)} = \tan^{-1}\frac{\mathcal{I}\{w_k'\}}{|x_k| + \mathcal{R}\{w_k'\}} - \frac{\mathcal{I}\{w_k'\}}{|x_k|},$$

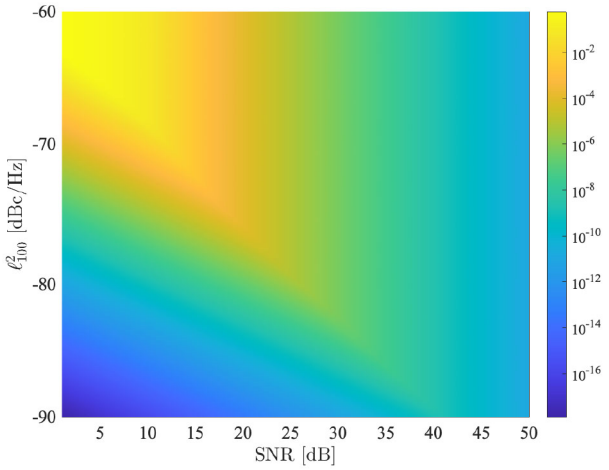

FIGURE 3. Normalized variance of the approximation error for the auxiliary channel models on which the design of the phase estimator is based.

and compute

$$\eta_k^{(i)} = \text{var}(e_k^{(i)})/\text{var}(n_k^{(i)}) \tag{81}$$

The variance of the noise sequence in the above equation is time-varying since it depends on $|x_k|$, and for this reason we average it over the transmitted symbols. In Figure 3, we report the minimum for $i = 1, 2$ of the normalized variance of the error, $\min\{\eta_k^{(1)}, \eta_k^{(2)}\}$ as a function of the SNR and ℓ^2_{100}.In the case of the high SNR approximation, the variance is independent of the PN parameters, while for the low PN approximation the PN sequence has been generated according to the following parameters: $R_s = 1$ MHz, $f_{3\text{dB}} = 10$ kHz and $\ell^2_\infty = -120$ dBc/Hz. From the figure, it can be seen that for all points the approximation error is very small, except for a region, the light yellow one, where neither of the two approximations works, being the PN particularly strong and the SNR low. It is worth noticing that a normalized error of 10^{-2} is already very low and corresponds to a system dominated by AWGN.

In the rest of the paper, we will denote by d_k and n_k the samples that we use for the phase estimation and the noise, respectively, leaving out the apex for simplicity.

B. RESIDUAL ERROR AFTER PHASE TRACKING

In this section, the optimal phase tracker is defined, based on the model above. Due to its nature, the noise θ_k^f in (27) cannot be tracked and hence it will be treated as additional AWGN for the derivation of the phase tracker and its variance added to the variance of the residual error. The optimal filter is derived in the hypothesis that the transmitted symbols are known (data-aided estimator). To make the analysis feasible, the focus is on a time-invariant estimator, by which the estimate of the PN samples, $\hat{\theta}_k$, can be obtained as the output of a linear time-invariant noncausal filter, i.e., the noncausal

Wiener filter, with input d_k and impulse response q_i [30], that is

$$\hat{\theta}_k = \sum_{i=-\infty}^{\infty} q_i d_{k-i}. \tag{82}$$

The above assumptions may seem strong, but we will show in Section VII that the derived closed-form expressions can predict the behavior of practical PN estimators.

We now consider the noise affecting the observations d_k. In each time instant, the variance of n_k depends on the modulus of the transmitted symbol, $|x_k|$, therefore the sequence is non-stationary, and the optimal MMSE estimator for this case is a time-varying filter. In order to find the optimal time-invariant filter, we assume that the noise affecting the observations is n'_k with variance

$$\sigma^2_{n'} = \frac{\ell^2_\infty}{T_\mathrm{s}} + \beta\frac{\sigma^2_w}{2} \tag{83}$$

and PSD

$$S_{n'}(f) = \ell^2_\infty + \frac{\beta\sigma^2_w T_\mathrm{s}}{2} \tag{84}$$

where we included the contribution of the noise θ^f_k. The parameter β is greater than or equal to 1. Particularly, two cases can be identified: one with $\beta = 1$, the other with

$$\beta = \mathrm{E}_x\left\{\frac{1}{|x_k|^2}\right\}. \tag{85}$$

The case $\beta = 1$ is representative of the phase estimator that is able to exploit the knowledge of the transmitted symbols for determining the variance of the additive noise n_k, such as the Kalman smoother that will be considered in Section VII.

Finally, the system model that we use for the design of the optimal filter for PN tracking is

$$d_k = \theta^c_k + n'_k. \tag{86}$$

Assuming the model (86), the optimal time-invariant MMSE filter, i.e., the noncausal Wiener filter, for the estimation of the phase according to (82) has Z-transform [30]

$$\mathbf{Q}(z) = \frac{\mathbf{S}_{\theta^c}(z)}{\mathbf{S}_{\theta^c}(z) + \mathbf{S}_{n'}(z)} \tag{87}$$

where $\mathbf{S}_{\theta^c}(z)$ and $\mathbf{S}_{n'}(z)$ are the Z-transforms of the autocorrelation of the sequence θ^c_k and n'_k, respectively.

The PSD of the residual PN $e_k = \theta_k - \hat{\theta}_k$ in the bandwidth $[-1/2T_\mathrm{s}, 1/2T_\mathrm{s}]$ can be obtained by using the expression of the PSD of the noise n'_k given in (84) and the expression of the PSD of the PN θ^c_k, given in (1) with $\ell^2_\infty = 0$. We obtain

$$S_e(f) = \frac{10^{10}\ell^2_{100}}{\frac{2\cdot 10^{10}\ell^2_{100}}{2\ell^2_\infty + \beta\sigma^2_w T_\mathrm{s}} + f^2_{3\mathrm{dB}} + f^2} + \ell^2_\infty. \tag{88}$$

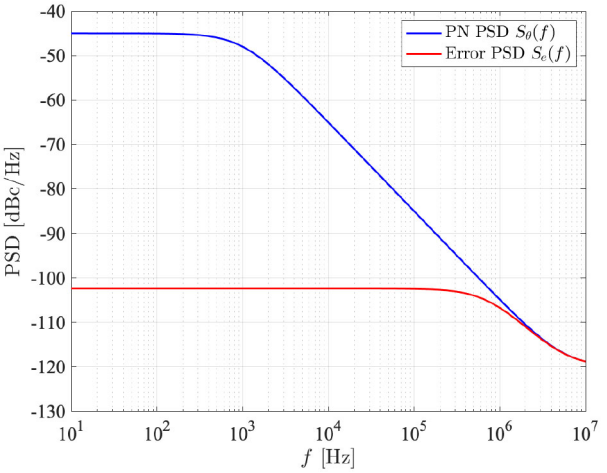

FIGURE 4. Power spectral densities of the phase noise and of the residual phase error after tracking in the system bandwidth.

From the above expression, we observe that the residual error PSD has the same shape of the PSD of the PN that we wish to estimate, with a 3dB bandwidth

$$\tilde{f}_{3\mathrm{dB}} = \sqrt{f^2_{3\mathrm{dB}} + \frac{2\cdot 10^{10}\ell^2_{100}}{\beta\sigma^2_w T_\mathrm{s} + 2\ell^2_\infty}}$$

larger than the one of the PN PSD. Figure 4 shows the two PSDs in the case where SNR = 10 dB, the PN is characterized by $\ell^2_{100} = -85$ dBc/Hz, $\ell^2_\infty = -120$ dBc/Hz, and $f_{3\mathrm{dB}} = 1$ kHz and the symbol rate is $R_\mathrm{s} = 10$ MHz.

The performance of a symbol-by-symbol detector, which ignores the correlation among symbols due to the residual PN, depends only on the first order statistics of the PN after tracking. For this reason, in the following we compute the variance of the residual PN error, which can be used to predict the performance of the considered system. Being the process zero-mean, the residual PN error variance, distorting the communication, is obtained by integrating the error spectrum in the communication bandwidth, that is

$$\begin{aligned}\sigma^2_e &= \int_{-\frac{1}{2T_\mathrm{s}}}^{\frac{1}{2T_\mathrm{s}}} S_e(f)df \\ &= \frac{2\cdot 10^{10}\ell^2_{100}}{\sqrt{f^2_{3\mathrm{dB}} + \frac{2\cdot 10^{10}\ell^2_{100}}{\beta\sigma^2_w T_\mathrm{s} + 2\ell^2_\infty}}}\mathrm{atan}\left(\frac{1}{2T_\mathrm{s}\sqrt{f^2_{3\mathrm{dB}} + \frac{2\cdot 10^{10}\ell^2_{100}}{\beta\sigma^2_w T_\mathrm{s} + 2\ell^2_\infty}}}\right) + \frac{\ell^2_\infty}{T_\mathrm{s}}.\end{aligned} \tag{89}$$

The expression above connects the phase error after tracking with the main PN parameters and with the system bandwidth. In the following, we derive simplified forms in the limiting case of *free-running* oscillator, i.e., $f_{3\mathrm{dB}} \to 0$, and study the impact of ℓ_∞ on the performance.

C. PERFORMANCE IN THE CASE OF FREE-RUNNING OSCILLATORS

In the case of *free-running* oscillators, i.e., $f_{3\text{dB}} \to 0$, the residual error variance is

$$\sigma_e^2 = \sqrt{2 \cdot 10^{10} \ell_{100}^2 (\beta \sigma_w^2 T_\text{s} + 2\ell_\infty^2)} \cdot \text{atan}\left(\frac{1}{2T_\text{s}} \sqrt{\frac{2 \cdot 10^{10} \ell_{100}^2}{\beta \sigma_w^2 T_\text{s} + 2\ell_\infty^2}} \right) + \frac{\ell_\infty^2}{T_\text{s}}. \quad (90)$$

By approximating the arctangent with $\pi/2$ and using the fact that $\beta \sigma_w^2 T_\text{s} \gg 2\ell_\infty^2$, the above expression becomes the following

$$\sigma_e^2 \simeq \pi 10^5 \ell_{100} \sigma_w \sqrt{\frac{\beta T_\text{s}}{2}} + \frac{\ell_\infty^2}{T_\text{s}}, \quad (91)$$

which can be also expressed in terms of the phase noise innovation variance given in (31), that is

$$\sigma_e^2 \simeq \sigma_u \sigma_w \sqrt{\frac{\beta}{8}} + \frac{\ell_\infty^2}{T_\text{s}}. \quad (92)$$

The above simplified expressions are useful for understanding how the residual PN scales with the system parameters. Regarding, for example, the symbol rate $R_\text{s} = 1/T_\text{s}$, if we consider that ℓ_∞ is usually very low, this result is in line with the observation that in most cases the performance improves if we increase the symbol rate, since the PN varies more slowly from one symbol to the other and hence it is easier to be tracked. On the other hand, there are cases where we observe the opposite behaviour, and this happens when the flat part of the PSD at high frequencies is not negligible. This means that the performance does not depend monotonically on the symbol rate. Particularly, the performance improves by increasing the symbol rate up to a point where the effect of the white phase noise entering the signal bandwidth dominates the performance.

Expression (91) can explain this phenomenon. The error variance in (91) is a concave function in $R_\text{s} > 0$ and hence its minimum can be computed by setting to zero the partial derivative with respect to R_s. In this way it is possible to find that the minimum of error variance is achieved in the symbol rate R_s^*

$$R_\text{s}^* = \left(\frac{\pi^2 10^{10} \ell_{100}^2 \beta \sigma_w^2}{8 \ell_\infty^4} \right)^{1/3}. \quad (93)$$

In Section VII, we will see that this result, although derived under the hypothesis of free-running oscillators, is useful also in the generic case of PLL oscillators.

VII. RESULTS

In this section, numerical results obtained through computer simulations are shown to validate our theoretical analyses.

TABLE 2. Parameters for the 3GPP PN model given in (94).

PSD0	3675 (35.65 dBc/Hz)			
n, m	$f_{z,n}$	$\alpha_{z,n}$	$f_{p,m}$	$\alpha_{p,m}$
1	3e3	2.37	1	3.3
2	451e3	2.7	1.54e6	3.3
3	458e6	2.53	30e6	1

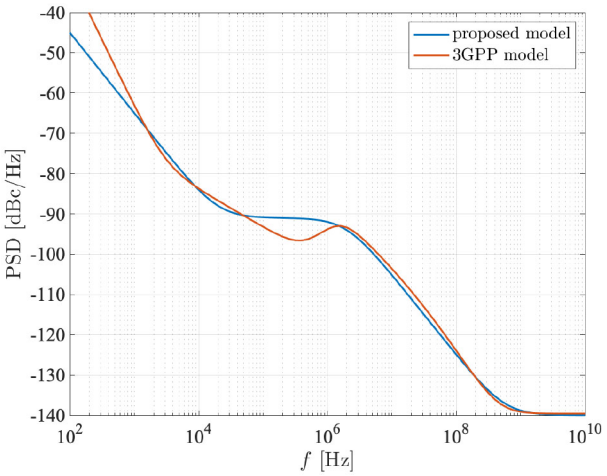

FIGURE 5. SSB power spectral density of the phase noise for a millimeter-wave frequency band, with carrier frequency of 45 GHz. The proposed model is obtained according to (5).

A. PHASE NOISE PSD MODEL FOR 3GPP PHASE NOISE

The proposed model is first compared with the multi-pole/zero model, by considering the PN typical of millimeter wave frequency band of next-generation cellular systems. The PN that can be found in the 3GPP documents [21], [22], whose single sideband (SSB) PSD is given by the following expression

$$S(f) = \text{PSD0} \frac{\prod_{n=1}^{N} 1 + \left(\frac{f}{f_{z,n}} \right)^{\alpha_{z,n}}}{\prod_{m=1}^{M} 1 + \left(\frac{f}{f_{p,m}} \right)^{\alpha_{p,m}}}, \quad (94)$$

is considered, where PDS0 is the value of $S(f)$ at $f = 0$. When the carrier frequency is 45 GHz, the parameters of the above PSD are given in Table 2, while the SSB PSD is shown in Figure 5. The spectrum is typical of a PLL-locked oscillator, where the PN at very low frequencies is due to the reference oscillator (see [10] for the description of PN of PLL systems). Figure 5 also shows the proposed model in the extended version (2), i.e., obtained as the sum of two independent processes, each one with PSD of the form (1), whose parameters are given in Table 3,[4] where the frequencies (low and high) where each process dominates are highlighted.

It is worth noticing that, starting from expression (94), it is difficult to derive a closed-form time-domain model for the PN, while the proposed approach leads to a very

[4]The parameters of the proposed model refer to the double sideband PSD of the phase noise.

TABLE 3. Proposed model: parameters for the two processes to follow the 3GPP PN spectrum.

low frequency		high frequency	
$f_{3\text{dB}}$	10 Hz	$f_{3\text{dB}}$	2e6 Hz
ℓ^2_{100}	-108 dBc/Hz	ℓ^2_{100}	-68 dBc/Hz
ℓ^2_{∞}	$-\infty$ dBc/Hz	ℓ^2_{∞}	-143 dBc/Hz

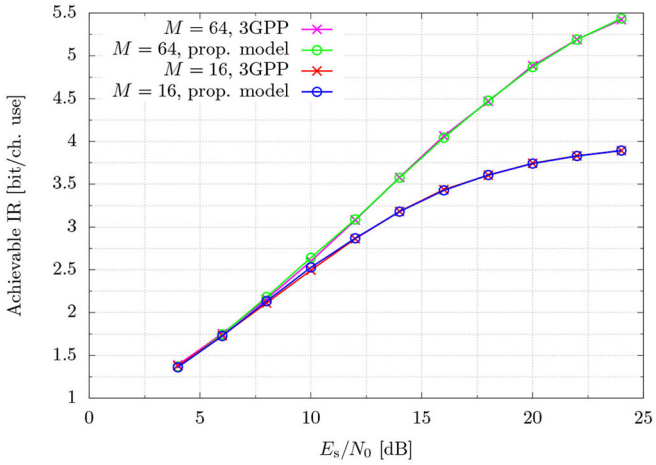

FIGURE 6. Achievable information rate for OFDM systems affected by PN generated according to the proposed model and the 3GPP model.

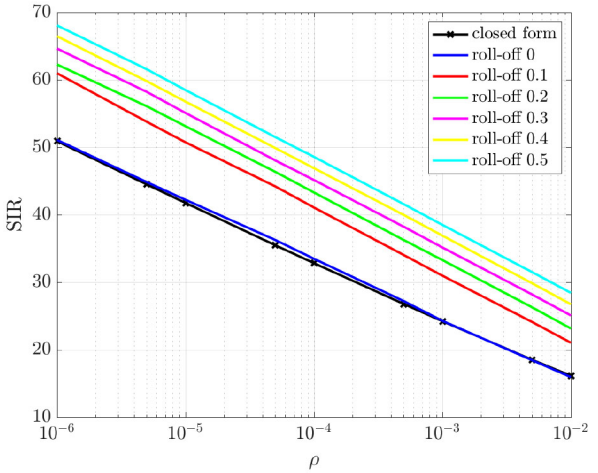

FIGURE 7. SIR after the matched filter at the receiver as a function of the relative bandwidth parameter ρ.

simple model for the time domain PN, that is the sum of two independent AR processes. This is at the expense of an approximation of the PSD. On the other hand, the deviation of the two models at low frequencies has no impact since the corresponding PN components are very slow and hence easy to track. In order to compare the performance of coded systems affected by the PN generated according to the two models (proposed and 3GPP), in Figure 6 we report the achievable information rate (IR) in bit per channel use for an OFDM system with 64-QAM and 16-QAM, using 1024 subcarriers with spacing 480 kHz, and with 800 active subcarriers. The fading is a Rayleigh process with realizations known at the receiver and constant over the OFDM symbol. For each OFDM symbol, the estimation of the CPE is based on the phases of the received samples at the pilot positions. The results show that the IR of the system using the proposed model for the PN is the same of the system using the 3GPP model for the PN.

B. VALIDATION OF THE ERROR ANALYSIS

We evaluate the SIR after the matched filter and the down-sampling operation of the continuous-time system in (24), simulated by using an oversampling factor 5. We consider the transmission of linearly modulated QPSK symbols with a RRC shaping pulse with roll-off factor ranging from 0 to 0.5. The simulated SIRs are reported as a function of the relative bandwidth parameter in Figure 7. In order to validate the proposed analysis, we report the curve that corresponds to the closed-form expression given in (42), that is obtained under the assumption that the filter $p(t)$ is the ideal sinc function (roll-off zero). The numerical results are in line with the closed-form analysis, being the simulated curve with roll-off zero almost overlapped with the theoretical one. Regarding the curves with roll-off larger than zero, they have the same behaviour and approach the closed form as the roll-off decreases.

In Figure 8, the hypothesis of constant channel gain is removed and we consider a Rayleigh fading channel with normalized Doppler bandwidth $f_D T_s$ ranging from 10^{-3} to $5 \cdot 10^{-2}$. The roll-off factor of the shaping pulse is 0.1 and the symbol time T_s is 10^{-5} s. The figure shows the SIR as a function of the bandwidth of the phasor $f_{3\text{dB},\phi}$, with the aim to compare the joint effect of PN and fading. It is worth noticing that, under the assumption of free-running oscillator and $\ell_\infty = 0$, the product $\rho = f_{3\text{dB},\phi} T_s$ fully describes the PN in the proposed model. The results show that for slow to medium fading, the SIR is mostly influenced by the PN, being the curves for $f_D T_s \leq 10^{-2}$ overlapped almost everywhere with the curve without fading. The curve for fast fading shows that in this case the fading dominates the performance.

The case of OFDM system is now considered. The effect of the ICI induced by the PN on the performance is evaluated by computing the achievable IR per channel use as a function of the per-carrier SNR. In Figure 9, a system with $N = 256$, $T_s = 10^{-6}$ s and 16-QAM is assumed. To focus on the ICI, the CPE is assumed to be perfectly compensated at the receiver. The achievable IR is computed by computer simulation for $\ell^2_{100} = -90$ dBc/Hz, $\ell^2_{\infty} = 0$ and for different value of $f_{3\text{dB}}$. These curves are compared with the ones representing the IR of an AWGN channel, where the SNR is computed through (63). The figure shows the match of the two curves for each case. The slight deviation at high SNR of the free-running oscillator curves is due to the suboptimality of the detector for the simulated curves. In fact, the employed detection algorithm is designed for an AWGN channel, without considering the ICI, which is taken

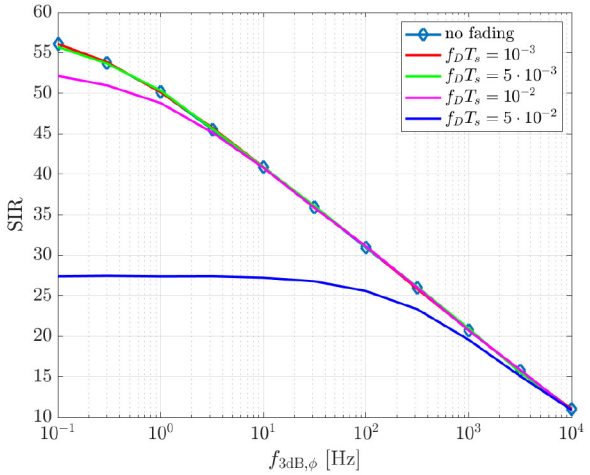

FIGURE 8. Signal-to-interference ratio after the matched filter at the receiver as a function of the phasor bandwidth for fixed T_s and for Rayleigh fading.

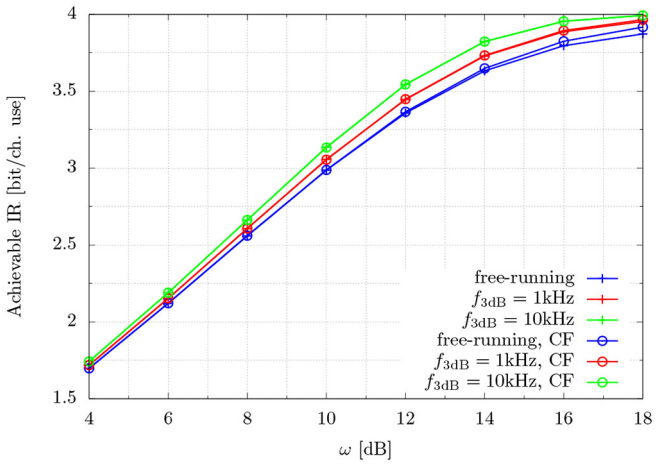

FIGURE 9. Achievable information rate in OFDM. Curves labeled CF represent the IR of an AWGN channel with SNR given by (63).

into account only through an increase of the noise variance, i.e., by assuming that the ICI is Gaussian.

C. OPTIMAL PHASE TRACKING THEORY

The analysis about the optimal phase tracking theory is validated by using computer simulations to compute the residual PN error after tracking. We consider the transmission of known 8-PSK symbols, i.e., pilot symbols, which are corrupted by PN and AWGN. The PN sequence has been generated according to the following parameters: $R_s = 500$ MHz, $f_{3\text{dB}} = 10$ kHz, $\ell^2_\infty = \{-120, -130\}$ dBc/Hz and $\ell^2_{100} = \{-80, -90\}$ dBc/Hz. At the receiver, the phase is estimated by exploiting the knowledge of the symbols. In Figure 10, the variance of the phase error after tracking obtained though simulation is reported and compared with the closed form (89), showing an excellent match between theory and numerical results. The figure also reveals the performance degradation due to the increase of ℓ^2_∞ and that this degradation is more prominent for

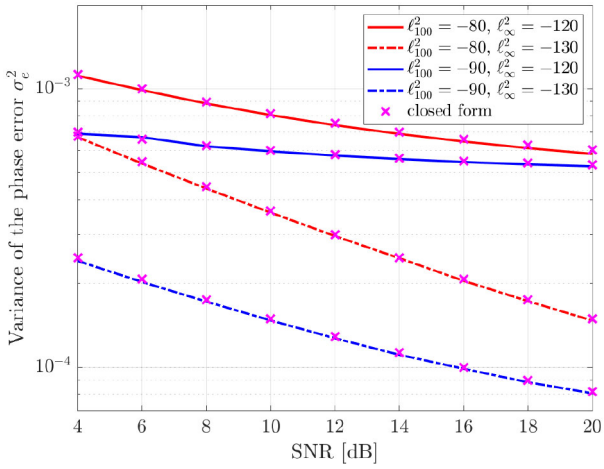

FIGURE 10. Variance of the phase error after tracking. Comparison between numerical results and closed form expression (89).

lower ℓ^2_{100}. Furthermore, for fixed ℓ^2_{100}, the dependence on the SNR is smaller when ℓ^2_∞ is larger, since the corresponding PN component cannot be tracked, even for very high SNR.

In the following, we study the performance of practical communication systems, where pilot symbols are inserted between fields of 50 information symbols. The simulation results are compared with the closed-form expression derived in Section VI. The PN sequence has been generated according to the following parameters: $R_s = 10$ MHz, $f_{3\text{dB}} = 10$ kHz, $\ell^2_\infty = -120$ dBc/Hz and $\ell^2_{100} = \{-80, -90\}$ dBc/Hz. At the receiver, after down conversion, the phase is estimated by using a practical PN estimator, that is a Kalman smoother [31], [32]. The Kalman estimator is employed in an iterative fashion: at the first iteration, the estimator uses only the pilots symbols, while in the successive ones it also uses the hard decisions on the information symbols and, since it uses the knowledge of the modulus of the symbols (exact/approximated in the case of pilots/information symbols), we set $\beta = 1$ in (89).

First we analyze the performance of an uncoded scheme with 8-PSK modulation. Figure 11 shows the variance of the phase error as a function of the SNR. The curves of the practical estimator follow the ones obtained in closed form after a given SNR, that corresponds to the SNR where the decisions fed back from the detector to the phase tracker are more reliable and hence the Kalman estimator is effective.

We now consider coded schemes using low-density parity-check (LDPC) code [33], with codeword size 64800 bits and rate 1/2. The coded bits are mapped into 16-QAM or 8-PSK. The Kalman smoother is run for 3 iterations and uses the hard decisions, obtained by running the detection and LDPC decoding algorithms. In Figures 12 and 13, we report the variance of the phase error as a function of the SNR for $\ell^2_{100} = -80$ and -90 dBc/Hz, respectively. Also in the coded case, the curves of the practical estimator match the closed form after a given SNR, that corresponds to the SNR where

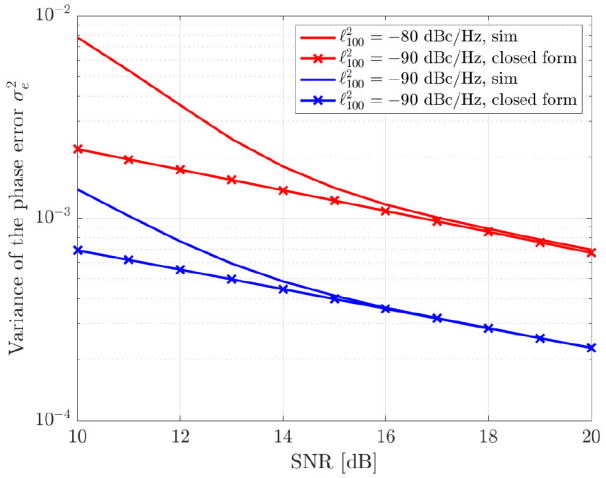

FIGURE 11. Variance of the phase error after tracking. Comparison between the practical Kalman-based estimator and the proposed closed-form expression in the uncoded transmission case.

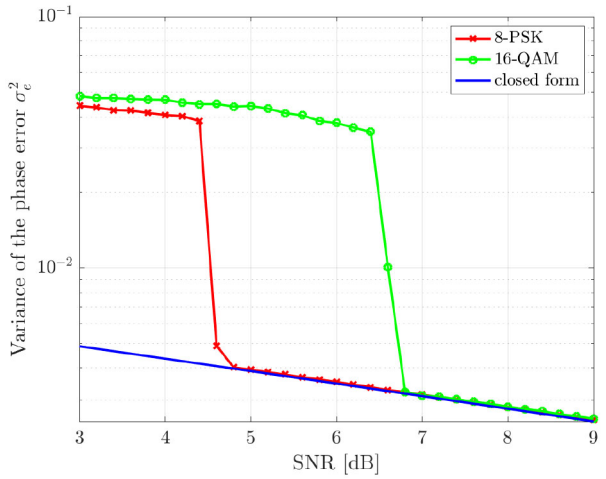

FIGURE 12. Variance of the phase error after tracking. Comparison between the practical Kalman-based estimator and the proposed closed-form expression for $\ell^2_{100} = -80$.

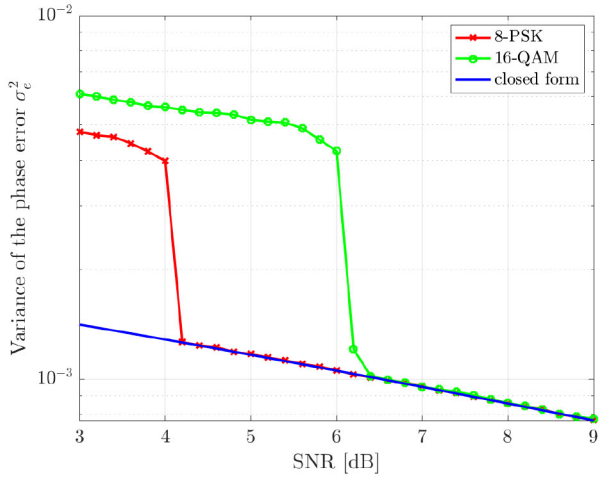

FIGURE 13. Variance of the phase error after tracking. Comparison between the practical Kalman-based estimator and the proposed closed-form expression for $\ell^2_{100} = -90$.

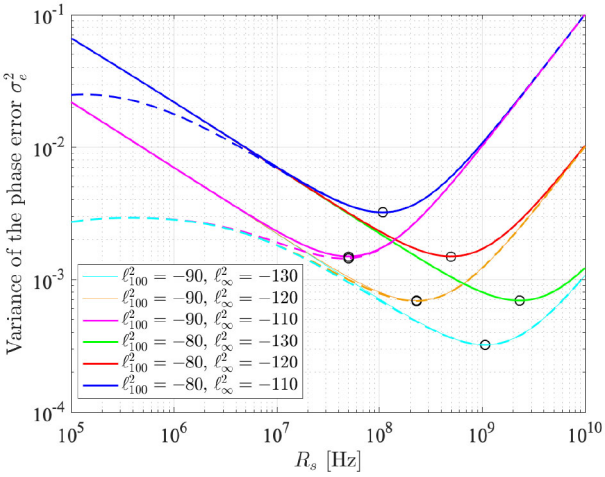

FIGURE 14. Error variance as a function of the symbol rate for PLL (continuous line) and free-running (dashed line) oscillators. The minimum of the variance obtained through (93) is indicated by circles.

the decisions fed back from the decoder to the phase tracker are reliable. This confirms that the hypothesis of known symbols, under which the closed form of the error variance was obtained, is fulfilled with good approximation. It is worth noticing that, for fixed PN parameters, the gap between the SNR where the simulations correspond to the theory for 8-PSK and 16-QAM is around 2 dB. This corresponds to the SNR gap in the Shannon capacity curve between 1.5 and 2 [bps/Hz], that are the mutual information of 8-PSK and 16-QAM coupled with a binary code with rate 1/2, respectively.

In Figure 14, we consider the variance of the residual error computed through the proposed closed-form expression as a function of the symbol rate R_s for SNR $= 0$ dB, $\ell^2_\infty = \{-130, -120, -110\}$ dBc/Hz and $\ell^2_{100} = \{-80, -90\}$ dBc/Hz. The dashed line are for the PLL-case, with $f_{3\text{dB}} = 10$ kHz, while the continuous lines are for the free-running oscillator case. The figure shows that the variance decreases up to a point where increasing the symbol rate is not beneficial anymore. On the contrary, the performance degrades due to the presence of the white PN. We observe that this change of trend happens for lower symbol rate when ℓ^2_∞ is larger. In the figure we report with a circle the argmin of the error variance computed through (93), and show that this computation is accurate and valid for both free-running and PLL oscillators.

VIII. CONCLUSION

In this paper, the phase noise typical of local oscillators in communication systems has been considered. The discrete-time phase noise channel has been studied by using analytical models described by means of parameters linked to measurements. The intersymbol interference and the power loss due to the presence of phase noise, affecting the samples obtained by matched filtering and sampling, have been bounded.

Then, we have studied the performance of phase tracking algorithms. We have applied the optimal estimation theory to find an expression for the residual error variance after tracking as a function of the PN parameters, the AWGN variance and the system bandwidth. Moreover, we derived in closed form the expression for the optimal symbol rate that minimizes the estimation error variance. Simulation results based on a practical Kalman based estimator have validated the proposed theory.

An important implication of our work is that the derived closed-form expressions can be used in the design of receiver algorithms and for performance prediction, starting from the knowledge of some fundamental parameters that can be found from measurements of practical oscillators.

REFERENCES

[1] L. Tomba, "On the effect of Wiener phase noise in OFDM systems," *IEEE Trans. Commun.*, vol. 46, no. 5, pp. 580–583, May 1998.

[2] A. G. Armada, "Understanding the effects of phase noise in orthogonal frequency division multiplexing (OFDM)," *IEEE Trans. Broadcast.*, vol. 47, no. 2, pp. 153–159, Jun. 2001.

[3] S. Wu and Y. Bar-Ness, "OFDM systems in the presence of phase noise: Consequences and solutions," *IEEE Trans. Commun.*, vol. 52, no. 11, pp. 1988–1996, Nov. 2004.

[4] G. Colavolpe, A. Barbieri, and G. Caire, "Algorithms for iterative decoding in the presence of strong phase noise," *IEEE J. Select. Areas Commun.*, vol. 23, no. 9, pp. 1748–1757, Sep. 2005.

[5] A. Demir, "Computing timing jitter from phase noise spectra for oscillators and phase-locked loops with white and $1/f$ noise," *IEEE Trans. Circuits Syst. I, Reg. Papers*, vol. 53, no. 9, pp. 1869–1884, Sep. 2006.

[6] A. Spalvieri and L. Barletta, "Pilot-aided carrier recovery in the presence of phase noise," *IEEE Trans. Commun.*, vol. 59, no. 7, pp. 1966–1974, Jul. 2011.

[7] G. Colavolpe, "Communications over phase noise channels: A tutorial review," *Int. J. Satell. Commun. Netw.*, vol. 32, pp. 167–185, May/Jun. 2014.

[8] M. R. Khanzadi, D. Kuylenstierna, A. Panahi, T. Eriksson, and H. Zirath, "Calculation of the performance of communication systems from measured oscillator phase noise," *IEEE Trans. Circuits Syst. I, Reg. Papers*, vol. 61, no. 5, pp. 1553–1565, May 2014.

[9] G. Colavolpe, E. Conti, A. Piemontese, and A. Vannucci, "The difficult road of expectation propagation towards phase noise detection," in *Proc. IEEE Int. Conf. Commun.*, 2023, pp. 4640–4645.

[10] A. Piemontese, G. Colavolpe, and T. Eriksson, "A new analytical model of phase noise in communication systems," in *Proc. IEEE Wireless Commun. Netw. Conf.*, 2022, pp. 926–931.

[11] J. Tubbax et al., "Compensation of IQ imbalance and phase noise in OFDM systems," *IEEE Trans. Wireless Commun.*, vol. 4, no. 3, pp. 872–877, May 2005.

[12] C. Muschallik, "Influence of RF oscillators on an OFDM signal," *IEEE Trans. Consum. Electron.*, vol. 41, no. 3, pp. 592–603, Aug. 1995.

[13] P. Robertson and S. Kaiser, "Analysis of the effects of phase-noise in orthogonal frequency division multiplex (OFDM) systems," in *Proc. IEEE Int. Conf. Commun.*, 1995, pp. 1652–1657.

[14] H. Ghozlan and G. Kramer, "Models and information rates for Wiener phase noise channels," *IEEE Trans. Inform. Theory*, vol. 63, no. 4, pp. 2376–2393, Apr. 2017.

[15] L. Barletta and G. Kramer, "Signal-to-noise ratio penalties for continuous-time phase noise channels," in *Proc. Int. Conf. Cogn. Radio Orient. Wireless Netw. Commun.*, 2014, pp. 232–235.

[16] S. Mandelli, M. Magarini, A. Spalvieri, and S. Pecorino, "On discrete-time modeling of the filtered and symbol-rate sampled continuous-time signal affected by Wiener phase noise," *Opt. Switch. Netw.*, vol. 18, pp. 96–103, Nov. 2015.

[17] J. Chen et al., "Does LO noise floor limit performance in multi-gigabit millimeter-wave communication?" *IEEE Microw. Wireless Compon. Lett.*, vol. 27, no. 8, pp. 769–771, Aug. 2017.

[18] J. Chen et al., "Influence of white LO noise on wideband communication," *IEEE Trans. Microw. Theory Tech.*, vol. 66, no. 7, pp. 3349–3359, Jul. 2018.

[19] A. Piemontese, G. Colavolpe, and T. Eriksson, "A new discrete-time model for channels impaired by phase noise," in *Proc. IEEE Glob. Telecommun. Conf.*, 2021, pp. 1–6.

[20] A. Mehrotra, "Noise analysis of phase-locked loops," in *IEEE/ACM Int. Conf. Comput. Aided Des. (ICCAD) IEEE/ACM Tech. Dig.*, 2000, pp. 277–282.

[21] "Study on new radio access technology: Radio frequency (RF) and co-existence aspects; Version 14.2.0," 3GPP, Sophia Antipolis, France, Rep. TR 38.803, 2017.

[22] "On mm-wave phase noise modelling," 3GPP, Sophia Antipolis, France, Rep. R4-1701165, 2017.

[23] L. Piazzo and P. Mandarini, "Analysis of phase noise effects in OFDM modems," *IEEE Trans. Commun.*, vol. 50, no. 10, pp. 1696–1705, Oct. 2002.

[24] J. R. Barry and E. A. Lee, "Performance of coherent optical receivers," *Proc. IEEE*, vol. 78, no. 8, pp. 1369–1394, Aug. 1990.

[25] G. J. Foschini and G. Vannucci, "Characterizing filtered lightwaves corrupted by phase noise," *IEEE Trans. Inf. Theory*, vol. 34, no. 6, pp. 1437–1448, Nov. 1988.

[26] M. Kline, *Calculus: An Intuitive and Physical Approach*. Chelmsford, MA, USA, Courier Corp., 1998.

[27] A. G. Armada and M. Calvo, "Phase noise and sub-carrier spacing effects on the performance of an OFDM communication system," *IEEE Commun. Lett.*, vol. 2, no. 1, pp. 11–13, Jan. 1998.

[28] D. Petrovic, W. Rave, and G. Fettweis, "Effects of phase noise on OFDM systems with and without PLL: Characterization and compensation," *IEEE Trans. Commun.*, vol. 55, no. 8, pp. 1607–1616, Aug. 2007.

[29] O. Edfors, M. Sandell, J.-J. Van De Beek, S. K. Wilson, and P. O. Borjesson, "OFDM channel estimation by singular value decomposition," *IEEE Trans. Commun.*, vol. 46, no. 7, pp. 931–939, Jul. 1998.

[30] J. Proakis, *Digital Communication*, 3rd ed., New York, NY, USA: McGraw-Hill, 1996.

[31] S. M. Kay, *Fundamentals of Statistical Signal Processing: Estimation Theory*. Upper Saddle River, NJ, USA: Prentice-Hall, 1993.

[32] L. Barletta, M. Magarini, and A. Spalvieri, "Bridging the gap between Kalman filter and Wiener filter in carrier phase tracking," *IEEE Photon. Technol. Lett.*, vol. 25, no. 11, pp. 1035–1038, Jun. 2013.

[33] "Digital Video Broadcasting (DVB); second generation framing structure, channel coding and modulation systems for broadcasting, interactive services, news gathering and other broadband satellite applications, Part II: S2-extensions (DVB-S2X)," ETSI, Sophia Antipolis, France, Rep. 302 307-2. Accessed: 2021. [Online]. Available: http://www.etsi.org

AMINA PIEMONTESE (Member, IEEE) received the Dr.Ing. degree in telecommunications engineering from the University of Parma, Italy, in 2006, and the Ph.D. degree in information technology from the University of Parma and TELECOM Bretagne, Brest, France, in 2011. From 2011 to 2015, she was a Postdoctoral Fellow with the Department of Engineering and Architecture, University of Parma, where she is currently an Associate Professor. From May 2015 to May 2020, she was with the Department of Electrical Engineering, Chalmers University of Technology, Gothenburg, Sweden. Her research activity includes various topics in digital communications, with particular emphasis on iterative joint detection and decoding algorithms, multiuser communications theory, and information theory. She received the Best Paper Award at the 5th Advanced Satellite Mobile Systems Conference and 11th International Workshop on Signal Processing for Space Communications 2010 and the IEEE Wireless Communications and Networking Conference, and the Marie Curie Individual Fellowship of the European Commission.

GIULIO COLAVOLPE (Senior Member, IEEE) received the Dr.Ing. degree (cum laude) in telecommunications engineering from the University of Pisa, Italy, in 1994, and the Ph.D. degree in information technologies from the University of Parma, Italy, in 1998. Since 1997, he has been with the University of Parma, where he is currently a Professor of Telecommunications with the Dipartimento di Ingegneria e Architettura. In 2000, he was a Visiting Scientist with Institut Eurécom, Valbonne, France. In 2013, he was a Visiting Scientist with the European Space Agency (ESTEC), Noordwijk, The Netherlands. His research interests include the design of digital communication systems, adaptive signal processing (with particular emphasis on iterative detection techniques for channels with memory), channel coding, and information theory. His research activity has led to more than 200 papers in refereed journals and in leading international conferences, and 18 industrial patents. He received the Best Paper Award at the 13th International Conference on Software, Telecommunications and Computer Networks, Split, Croatia, September 2005, the Best Paper Award for Optical Networks and Systems at the IEEE International Conference on Communications, Beijing, China, May 2008, and the Best Paper Award at the 5th Advanced Satellite Mobile Systems Conference and 11th International Workshop on Signal Processing for Space Communications, Cagliari, Italy, 2010. He served as an Editor for IEEE TRANSACTIONS ON WIRELESS COMMUNICATIONS, IEEE TRANSACTIONS ON COMMUNICATIONS, and IEEE WIRELESS COMMUNICATIONS LETTERS and an Executive Editor for *Transactions on Emerging Telecommunications Technologies*.

THOMAS ERIKSSON received the Ph.D. degree in information theory from the Chalmers University of Technology, Gothenburg, Sweden, in 1996. From 1990 to 1996, he was with the Chalmers University of Technology. In 1997 and 1998, he was with AT&T Labs-Research, Murray Hill, NJ, USA. In 1998 and 1999, he was with Ericsson Radio Systems AB, Kista, Sweden. Since 1999, he has been with the Chalmers University of Technology, where he is currently a Professor of Communication Systems. Further, he was a Guest Professor with Yonsei University, South Korea, from 2003 to 2004. He is currently the Vice Head of the Department of Signals and Systems, Chalmers University of Technology, where he is responsible for undergraduate and master's education. He has authored or coauthored more than 250 journal and conference papers, and holds 14 patents. He is leading the research on hardware-constrained communications with the Chalmers University of Technology. He is currently leading several projects on, e.g., massive MIMO communications with imperfect hardware; MIMO communication taken to its limits: 100-Gb/s link demonstration; mm-Wave MIMO testbed design; satellite communication with phase noise limitations; and efficient and linear transceivers. His research interests include communication, data compression, and modeling and compensation of nonideal hardware components (e.g., amplifiers, oscillators, and modulators in communication transmitters and receivers, including massive MIMO).

Open Access funding provided by 'Università degli Studi di Parma' within the CRUI CARE Agreement